Per-Unit Hysteresis and Eddy Loss Method Based on 3D Finite Elements for Non-Symmetric Toroidal Magnetic

JORGE RAFAEL GONZÁLEZ-TEODORO[ID]**1,**
ENRIQUE ROMERO-CADAVAL[ID]**1, (Senior Member, IEEE), AND RAFAEL ASENSI**[ID]**2**
[1]Department of Electrical, Electronic and Automatic, University of Extremadura, 06006 Badajoz, Spain
[2]Centro de Electrónica Industrial, Universidad Politécnica de Madrid, 28006 Madrid, Spain

Corresponding author: Jorge Rafael González-Teodoro (jordirgt@hotmail.com)

ABSTRACT Several main methodologies are used to estimate the core power loss (CPL) in magnetic components. One group is based in the Steinmetz equation (The modified one, the generalized one and the natural equations are the principals). Another one is the separation of losses between hysteresis, eddy current and excess losses. The third group is based mathematical-empirical hysteresis models and the last one is based on the magnetization process. These approaches need a prior test or analysis to calculate the CPL. Tests are usually expensive, or the number of needed tests is excessive for the component design process. 2D analyses are not enough for some magnetic components due to their lack of symmetries. Toroidal core components are ones of the most common components in transformers and power converters. They do not have symmetries in the magnetic field distribution and only 3D models are satisfactory to take into account all the effects and phenomena. An extensive study of 3D model finite element analysis was developed to determine the main losses in magnetic components core, the hysteresis and eddy current losses. A new methodology is presented, per-unit CPL (considering only Hysteresis and Eddy Current Losses) that permits analyzing the impact of the involved factors separately. The proposed per-unit CPL allows the definition of a new equation for determining hysteresis and eddy current losses using only the geometrical and material parameters (core and coils) used to estimate the total CPL.

INDEX TERMS Eddy current, Hysteresis loss, core power loss, 3D modeling, finite element analysis.

I. INTRODUCTION

Losses in magnetic cores have been studied because of their particular significance to component design. Physicists study the characteristics in magnetic materials, while design engineers in power electronics need to model the core power loss (CPL). Nevertheless, there is a gap between the power loss calculation theories, focused on material characteristics, and engineering applications. In consequence, the devices designed cannot fully use the material capabilities.

One set of models is based on the Steinmetz equation [1], where the three coefficients are determined by fitting the loss model to the measurement data. This model assumes purely sinusoidal flux densities. An extension of the Steinmetz equation was presented by Jordan in [2] for an iron loss

model where the static hysteresis loss (HL) and dynamic eddy current loss (ECL) were separated. Pry and Bean added the excess loss factor or anomalous factor [3]. Bertotti developed a theory to calculate losses by introducing the concept of magnetic objects, which led to excess loss in terms of the active magnetic objects and the domain wall motion [4], [5]. Once the separation of iron losses after the magnetizing processes was included, the losses caused by linear magnetization, rotational magnetization and higher harmonics were added [6], [7].

In recent decades, the Steinmetz equation was improved. The Modified Steinmetz equation was presented in [8] for arbitrary waveforms and the Generalized Steinmetz equation [9] presented the idea of the instantaneous iron loss as a single-valued function of the flux density and the rate of change of the flux density. The improved Generalized Steinmetz equation [10] was developed to avoid the limitation in

The associate editor coordinating the review of this manuscript and approving it for publication was Derek Abbott[ID].

the third higher harmonic. For rectangular shape voltages, the improved-improved generalized equation was introduced in [11].

To obtain higher accuracy, hysteresis models (Preisach and Jiles-Atherton) were developed [12], [13]. An improvement of the Preisach model was presented in [14] including a dynamic part divided into two sections describing the low and high values of the flux density. A friction hysteresis model based on an energy approach, where the magnetic dissipation from the macroscopic point of view is represented by a friction-like force, was introduced in [15]. Advances for nonlinear behavior were presented in [16]. A new model, which describes the switching behavior, was implemented in Matlab [17]. Analyses for non-sinusoidal signals for specific components have been developed in recent years [18], [21].

The empirical and separation loss models are preferable and best suited for fast and rough iron loss definition. The complex HL models are more suited for an exact iron loss. However, they need much more knowledge about the material data or prior material measurements as well as more information about the flux density waveforms. Another huge issue is integration into finite element tools. Most of the methods to calculate the CPL is necessary to obtain the magnetic field density in a previous analysis or test. If FEM is used to calculate the magnetic field density, the asymmetric components that need a 3D model, however due to the current computational limitations [21], [22] is a difficult task to achieve enough accuracy or it is not productive due the CPU time. The proposed methodology gives an original equation to determine the CPL for Toroidal components used in switched-mode power supplies (normally in non-saturation status) for any signal-based 3D finite element analyses (FEA) [23].

The analyses in Maxwell were developed in transient solver [24], where it is able to introduce the hysteresis data as a loop (non-linear data) from a frequency range from 1 Hz to 1209 MHz. The material properties of the material have been selected also in the Model and the Mesh has been automatic generated (1% error and 25 maximum number of passes, step refinement of 20%). The excitations (input and output) has been introduced in sheets created into the windings. The non-linear data for the hysteresis data [26] (not only the permeability) was introduced in the pre-modelling phase. developing geometrical (for the core and the windings) and material permutations at different operation frequencies and covering all this range to achieve a final equation to calculate the CPL for every toroidal core component.

This research based on 3D FEM allows to obtain a new equation (without needing use FEM) in order that the power engineers don't need to use any previous analyses to obtain the magnetic field, and only using the geometrical and material properties of the winding (including the waveform) and the core can determinate a loss estimation, being very useful for the optimization process for the power designers.

A brief description of the CPL is shown in Section 2. The following section explains the original contribution (per-unit CPL) which is the tool for this research. Sections 4–5 contain the analysis sequences using FEA for HL and ECL. The paper finishes with the validation of the proposed equations.

II. CORE POWER LOSS

The CPL is mainly classified into two types: HL and ECL. Other losses such the excess losses are attributed to the peculiar nature of nonlinear electromagnetic field diffusion in the lamination for the magnetic core. They are due to the non-uniform profiles of magnetic flux and they are calculated into the eddy current in the FEM [27].

$$P_t = P_{\text{hysteresis}} + P_{\text{eddy}} \qquad (1)$$

The magnetization and demagnetization of the magnetic core in each AC cycle cause an energy loss named HL. This energy loss depends on the properties of the specific core material and is proportional to the hysteresis loop area.

$$P_{\text{hysteresis}} = \int_{\text{vol}} \frac{1}{2} \cdot \omega \cdot \text{Im}\left(\vec{B} \cdot \vec{H}^*\right) dV \qquad (2)$$

where $\vec{B}$ is the magnetic flux density, $\vec{H}^*$ is the complex conjugate of the magnetic field and ω is the angular frequency.

ECL is caused by an electric current increase due to the alternating magnetic field. These losses arise from the fact that the core itself is composed of conducting material so that the voltage induced in it by the varying flux produces circulating currents in the material. ECL depends upon the rate of change of flux as well as the resistance of the path; it is reasonable to expect this loss varies as the square of both the maximum flux density and frequency if the core is solid and made up from ferromagnetic materials, and it effectively acts as a single short-circuited turn. Induced eddy currents, therefore, circulate within the core in a plane normal to the flux and cause resistive heating in the core material [26].

$$P_{\text{eddy}} = \int_{\text{vol}} \frac{1}{2\sigma} \cdot \left(\vec{J} \cdot \vec{J}^*\right) dV \qquad (3)$$

where $\vec{J}$ is the current density, $\vec{J}^*$ is the complex conjugate of the current density and ω is the conductivity in a structure.

III. PER-UNIT CPL

The CPL analysis was performed with the original methodology based on the concept named per-unit CPL:

$$\frac{P_i}{P_1} = P_{p.u.} \qquad (4)$$

where P_i is the CPL of any toroidal core model in a particular frequency and P_1 is the CPL for the reference component (RC) at the same frequency.

Any component could have been selected as RC and the conclusions would have been the same since the results were obtained by normalization. The definition of the per-unit CPL permits calculating the effect of each analysed parameter independent from the frequency. Frequency independence gives the tool the ability to analyse each loss parameter using FEM parametric analyses.
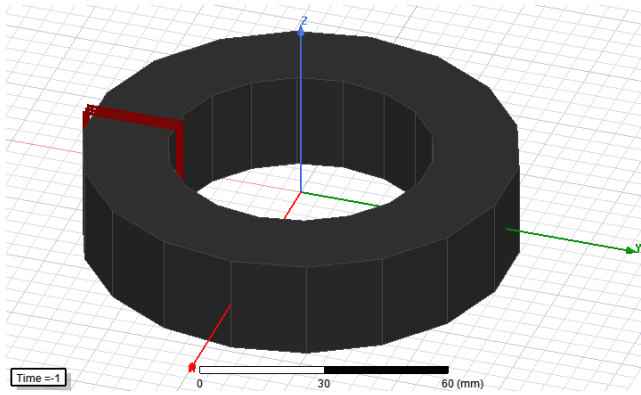
FIGURE 1. Reference component (C.107.65.25) with 1 winding (AWG 24).

For the HL study, the RC was a Toroidal component C107.65.25 (see dimensions in [26]) with 1 winding (4 turns with 1° lateral distance) and 3C90 core material. For the ECL, the RC was a Toroidal component C107.65.25 with 1 winding (3 turns with 1° lateral distance) and 3F3 core material (Fig. 1).

IV. HYSTERESIS POWER CORE LOWER LOSS

The per-unit CPL was used for the hysteresis study using several analysis sequences. The analysis consists of comparing the HL defined in (2) from the RC to other, different models only changing a specific parameter by sequence to investigate the parameter's impact on the HL. The first parameter in these analysis sequences is the core material. See Table 1 for the materials, with different permeabilities, coercivities and hysteresis loop areas, used so that these analyses cover the materials range used in power electronics.

To model the HL, the hysteresis loop of the material is introduced in the ANSYS Maxwell Transient solver using data from the Ferroxcube datasheet [26]. To do this, a table with enough points (48) to describe the hysteresis loop in a piecewise linear mode is introduced in the assistant tool in the pre-modeling. In eddy current solver is only available the linear permeability, this is the reason that the transient solver has been chosen.

The results of the per-unit CPL modifying the material are plotted in Fig. 2. The results demonstrate that the per-unit CPL is constant independent of the frequency for each material.

Figure 3 demonstrates that the HL is proportional to the hysteresis loop as the theory predicts (5). This conclusion demonstrates that the scripts used in the FEA tool for the HL were properly used.

$$P_{p.u} = \frac{P_i}{P_1} = \frac{S_i}{S_1} = S_{p.u.} \tag{5}$$

where S_i is the surface of the hysteresis cycle from component i and S_1 is the surface of the hysteresis loop for the RC.

The hysteresis loop areas were calculated from [28] with approximations using a 6th order polynomial. The small discrepancies with materials 4A11 and 3F4 are because their
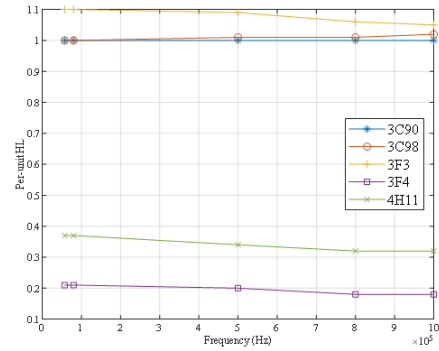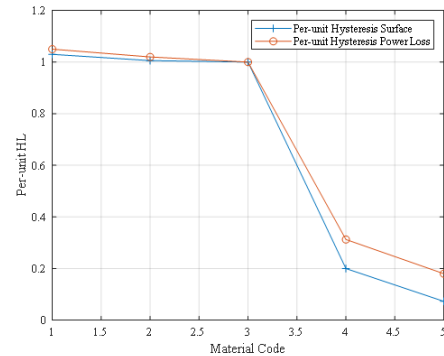

FIGURE 2. Per-unit HL vs core material.

FIGURE 3. Per-unit HL vs per-unit hysteresis loop area.

TABLE 1. Material properties.

Code	Mater.	B (mT)	H (A/m)	μr	Bmax (mT)	H_{max} (A/m)	Energy (J) (Hysteresis loop area)	Proportion	Maximum frequency in datasheet (kHz)
1	3F3	152	18	4000	410	250	429056	1,05	600
2	3C98	138	17	5000	450	275	426048	1,02	700
3	3C90	160	19	5500	435	250	423669	1,00	900
4	4A11	110	32	850	325	1000	43083	0,31	1000
5	3F4	155	66	1700	407	1000	30928	0,18	1500

hysteresis loops are narrow and higher-order mathematical approximations are needed. The hysteresis loop data from [26] is for 25°C, but Equation (5) is also valid for different temperatures. The loop area Si for a different temperature can be calculated following the manufacturer's instructions and our coefficients for the loop surface are calculated as indicated above. The RC continues being the same S1 as for 25°C and the CPL is calculated using (5) at the new temperature.

The analyses have been developed from 1 to 1200 kHz, using the parameters given by manufacturers in their corresponding material datasheets, that are valid for frequency lower than the maximum indicated in Table 1, over this frequency, these values should be updated. In this work, it has been decided not to update these values, because no information is given by manufactures on how to do it and the switching operation frequency of converters based on Si,
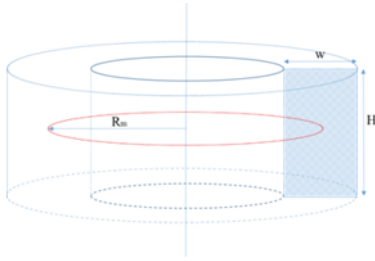
FIGURE 4. The toroidal core volume.

TABLE 2. Per-unit CPL.

Volume (mm^3)	Change in dimensions related to standard core (mm)		Frequency (kHz)			
			500	133.3	80	57.1
0.176	None		1	1	1	1
0.169	Height	(-1)	0.98	0.97	0.97	0.97
0.168	Width	(-1)	0.97	0.97	0.97	0.97
0.162	Height	(-2)	0.94	0.93	0.93	0.93
0.16	Height	(-3)	0.89	0.90	0.90	0.90
0.155	Width	(-2)	0.91	0.91	0.91	0.91
0.151	Width	(-3)	0.87	0.87	0.87	0.86

SiC or GaN semiconductors are usually bellow the maximum frequencies indicated in Table 1.

A. CORE VOLUME EFFECT
The core volume was calculated following (6) for toroidal cores and the volume can be modified independently through height, width and radius. Where R_m is the main radius of the toroidal core and A is the surface area of the cross-section ($A = wH$) (Fig 4).

$$V = 2 \cdot \pi \cdot R_m \cdot A \qquad (6)$$

Two analysis sequences were launched. One sequence was to modify the height and width from the RC. The per-unit CPL was constant independent of the frequency and the per-unit CPL was equal to the per-unit volume. The values of the per-unit CPL (under core volume sequence) are shown in Table 2. Figure 5 shows the relationship between the per-unit CPL and the per-unit core volume. This correlation is defined by (7).

$$\frac{P_i}{P_1} = \frac{V_i}{V_1} = \frac{2 \cdot \pi \cdot R_m \cdot A_i}{2 \cdot \pi \cdot R_m \cdot A_1} = \frac{w_i \cdot H_i}{w_1 \cdot H_1} \qquad (7)$$

where V_i is the volume of the toroidal core for component i and V_1 is the volume for the RC. Another sequence consists of the main radius permutation for the toroidal component being constant at the cross-section. Equations (8) and (9) define the results showed in Fig. 6, where there are two different scenarios.

$$\frac{P_i}{P_1} = \left(\frac{2 \cdot \pi \cdot R_i \cdot A_1}{2 \cdot \pi \cdot R_1 \cdot A_1} \right)^{-1.7} = \left(\frac{R_i}{R_1} \right)^{-1.7} \qquad (8)$$

$$\frac{B_i}{B_{Sat}} \geq 1 \rightarrow \frac{P_i}{P_1} = \left(\frac{2 \cdot \pi \cdot R_i \cdot A_1}{2 \cdot \pi \cdot R_1 \cdot A_1} \right)^{-2.95} = \left(\frac{R_i}{R_1} \right)^{-2.95} \qquad (9)$$

In the first, when the core is not saturated, the correlation follows (8). The second, when the core is in saturation
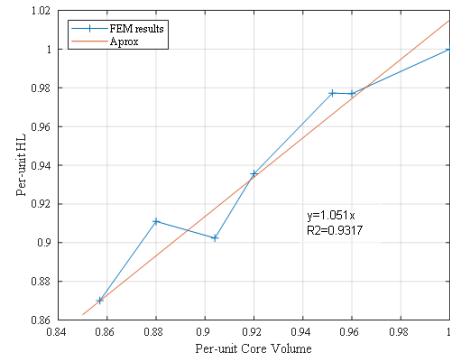

FIGURE 5. The per-unit HL vs normalized core volume.
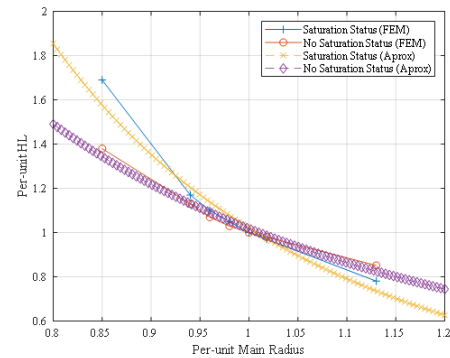

FIGURE 6. Per-unit HL vs per-unit main radius.

($B_i \geq B_{max}$) is according to (9). See Fig. 6 to compare the different behaviours. The exponents used in (8) and (9) were obtained from mathematical regressions from the developed permutations.

B. WINDING CURRENT EFFECT
The per-unit CPL (under winding current sequence) is shown in Fig. 7. The per-unit CPL was constant in the practical current range for the components used in power electronics. If the current is in this range, the relationship agrees with (10).

$$\frac{P_i}{P_1} \sim \left(\frac{I_i}{I_1} \right)^{2.95} \qquad (10)$$

where I_i is the current for component i and I_1 is the current for the RC. In theory, with the FEA tool, we can analyse the case when the current is outside of the regular range (probably with the core in saturation); then, the relationship follows (11).

$$\frac{B_i}{B_{Sat}} \geq 1 \rightarrow \frac{P_i}{P_1} = 0.0002 \cdot f + \left(\frac{I_i}{I_1} \right)^{2.95} \cdot \left(\frac{S_i}{S_1} \right)^{\frac{1}{2}} \qquad (11)$$

These assumptions were checked with other materials, different winding geometries and configurations. As with the previous sequences, the exponents were obtained from mathematical regressions.

C. NUMBER OF TURNS EFFECT
This analysis sequence modifies the number of turns in the winding (The RC has 4 turns). The same geometric parameters were applied for the windings. The effects from the
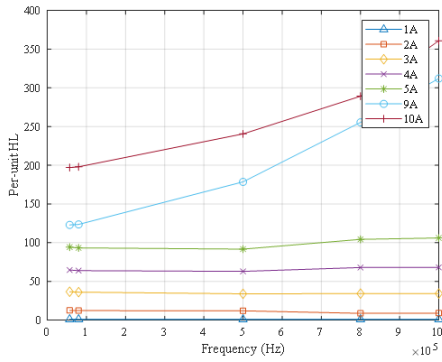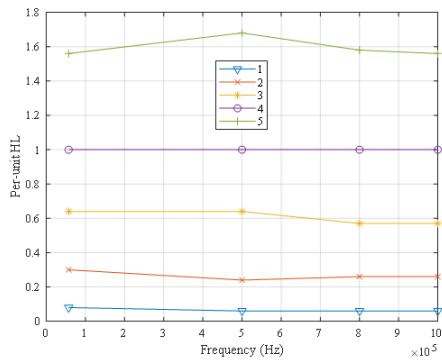
FIGURE 7. Per-unit HL vs freq. (current).

FIGURE 8. Per-unit HL vs freq. (turns).

FIGURE 9. Per-unit HL vs current.

FIGURE 10. Per-unit HL vs wiring diameter.

winding geometric configuration are analysed further in next analyses sequences. As with the other sequences, the per-unit CPL was uniform in the frequency range, which permits us to give the following relationship (Fig. 8):

$$\frac{P_i}{P_1} = 0.06 \cdot \left(\frac{n_i}{n_1}\right)^2 \tag{12}$$

where n_i is the number of turns for component i and n_1 is the number of turns for the RC.

D. SEVERAL WINDING EFFECT
These analyses were developed based on the RC (inductive component with only one winding). This analysis sequence serves to compare the difference between components with one or several windings.

An additional winding was added to the RC. The additional winding has 4 turns (diameter AWG 18) with the same lateral distance as the former coil (diameter AWG24). AWG18 was chosen because the skin effect is double that of AWG24. The FEA simulation was performed under open circuit status. Thus, the component works as an inductive component. However, the effect of copper wiring around the winding could be analysed in this sequence. Fig. 8 shows the studied configurations (the diameters in the different cases were modified as well for other sequences). The relationship between the per-unit CPL and frequency is defined for the three cases (inductive component, only from the 1° winding and only
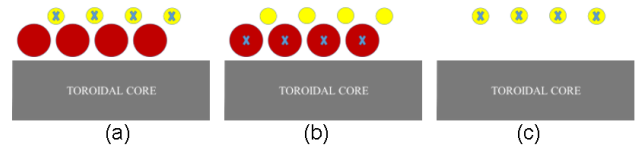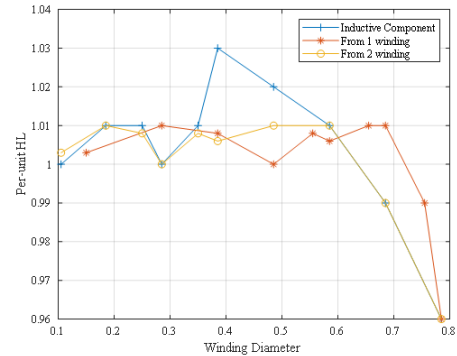
from the 2° winding). Equation (14) defines that the impact for having copper wires without current is negligible from the core loss point of view.

(a) From 1° winding (b) From 2° winding (c) Referenced Component

The impact of the winding configuration in the CPL is about 5% compared with the material, volume and other parameters (Fig. 10) in normalization data.

E. WINDING CONFIGURATION EFFECT
Another important set of analyses were studied for different winding configurations for the magnetic component. The winding cross-section has an impact on the CPL in the case that the diameter is huge for inductive components because some magnetic field densities are spread into the wires instead of the core. Nevertheless, the effect is negligible for the diameters used for regular manufactured magnetic components. In addition, if the diameter is less than 2.4 times d1 (diameter for the RC), the effect is non-existent.

The winding position at the toroidal core is not expected to have any effect on the HL (Fig. 10). The lateral distance between windings has a minimal effect to consider (the analysis was developed with a constant lateral distance between turns in the winding). This effect is ruled by (13).

$$\frac{P_i}{P_1} = e^{-0.004 \cdot \alpha} \tag{13}$$

where α is the angle between turns (degree) in the same winding from the vertical axis at the centre of the magnetic component. See Fig. 11. The impact is negligible for standard/commercial windings configurations.

The 4 lateral distances for the winding configuration (vertical or horizontal between the turn edges and the core, Fig. 12)
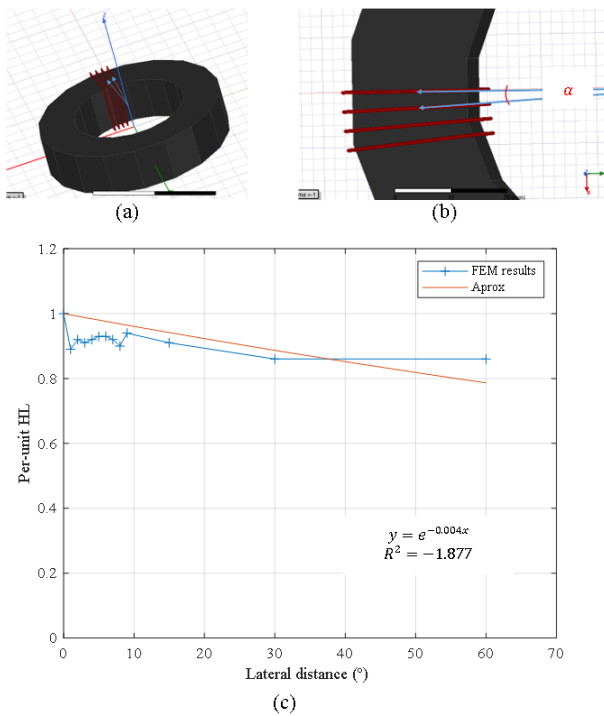
FIGURE 11. Per-unit HL vs lateral distance.

TABLE 3. Variations of the winding geometry.

Per-unit Vertical Distance	Per-unit CPL									
	1.00	1.03	1.05	1.10	1.13	1.17	1.21	1.28	1.7	3.37
500000 Hz	1.00	1.02	0.99	1.00	0.98	1.01	1.00	1.00	0.9	1.00
133333.3 Hz	1.00	1.01	1.01	1.01	0.99	1.03	1.02	1.01	1.0	1.02
80000 Hz	1.00	1.01	1.01	1.01	0.99	1.03	1.02	1.01	1.0	1.02
57142.85 Hz	1.00	1.01	1.01	1.01	0.99	1.03	1.02	1.01	1.0	1.02
AVERAGE	1.00	1.01	1.01	1.01	0.99	1.03	1.02	1.01	1.0	1.02

TABLE 4. Variations of the winding geometry different diameter.

	Lateral Distance	1.60	2.00	2.20	2.60	3.00
	0.285	1.00	1.00	0.98	1.00	0.99
Diameter	0.385	0.99	1.01	1.00	1.02	1.00
	0.485	1.00	0.98	1.00	0.97	0.99
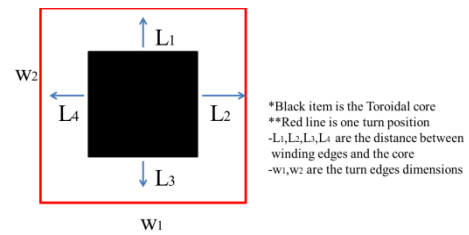
FIGURE 12. The winding geometry configuration.

could be modified independently with different values in the same winding. An important conclusion of this analysis sequence is that the per-unit CPL is similar if the sum of the vertical distances $(L_1 + L_3)$ has the same value for all potential configurations A similar conclusion is achieved for horizontal distances $(L_2 + L_4)$. See Table 3. The reason for this conclusion is that the magnetic field density does not suffer a significant variation inside the core. Even equivalent vertical or horizontal distances ~3.5 times larger than the RC do not have any impact on HL. Table 4 shows the results for per-unit CPL for similar analysis sequences with different diameters for the coil in the RC with similar results.

In summary, the winding configuration for regular inductive components with toroidal components did not impact the HL. The main factors are the core material, core volume, coil current and number of turns in the windings.

$$\frac{P_i}{P_1} = 1 \cdot f^{0.0035} \approx 1 \quad (14)$$

F. HYSTERESIS POWER CORE LOSS EQUATION

The relationship between P_i and P_1 (RC) for each involved parameter was established after the previous analysis sequences. The correlations obtained with the per-unit CPL, that has been checked for the analysed range of frequencies (1 Hz - 1200 kHz), permit defining an algorithm to predict the HL for toroidal components.

For inductive components, considering a constant lateral distance between windings and an unsaturated status, the HL

can be defined as:

$$P_{\text{oh}} = \left(\frac{0.05}{2} \cdot e^{-0.0004 \cdot \alpha}\right) \cdot \left(n_i^2\right) \cdot \left(I_i^{2.95}\right) \cdot V \quad (15)$$

$$P_{\text{ih}}(f) = P_{oh} \cdot f^{\text{exp}} \rightarrow \exp = \frac{0.0691}{S_1} \cdot S_i + 0.7926 \quad (16)$$

where P_{oh} is the HL for the magnetic component (1 Hz) and P_{ih} is the HL in the frequency working point desired. Using superposition theorem, the values of the core loss could be obtained when the toroidal component works with several windings. Superposition theorem can apply to magnetic fields and current densities. It is not applied to energies and losses due to a linear system are needed for the application. The non-linear part of a magnetic component, as far as current is concerned, is the core. However, in this case, the theorem for the magnetic field, based on [28], [29] is used for the current densities. Thus, if the toroidal core component has more than one winding, the hysteresis core loss is defined as:

$$P_{\text{oh}} = \left(\sum_j \frac{0.05}{2} \cdot e^{0.0004 \cdot \alpha_j}\right) \cdot \left(\sum_j \left(n_j^2\right) \cdot \left(I_j^{2.95}\right)\right) \cdot V \quad (17)$$

$$P_{\text{ih}}(f) = P_o \cdot f^{\text{exp}} \rightarrow \exp = \frac{0.0691}{S_1} \cdot S_i + 0.7926 \quad (18)$$

In the case of core saturation, the correlations defined in the previous analysis sequences allow defining a mathematical algorithm to predict the hysteresis core loss in the same way
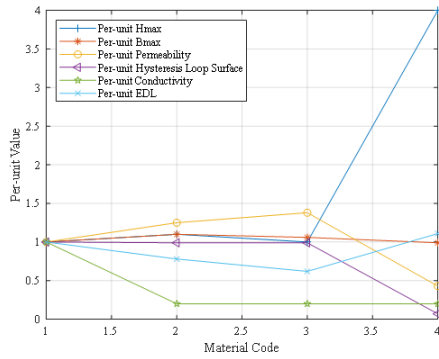
FIGURE 13. Per-unit EDL vs per-unit values.

TABLE 5. Material properties.

Code	Mater.	B (mT)	H(A/m)	μr	Bmax (mT)	H_{max} (A/m)	σ(1/p)(Ωm)
1	3F3	152	18	4000	410	250	0,50000
2	3C98	138	17	5000	450	275	0,10000
3	3C90	160	18.5	5500	435	250	0,10000
4	3F4	155	66	1700	407	1000	0,10000
5	4A11	110	32	850	325	1000	0,00001

that we have defined for the case without saturation but taking (9) and (11) into account.

V. EDDY CURRENT POWER CORE LOWER ANALYSIS

Several analysis sequences were launched using the per-unit CPL methodology as in the HL analysis. The only difference was that the RC used was modified as explained previously. The RC was a toroidal component, C107.65.25, with 1 winding (3 turns with 1° lateral distance) and 3F3 core material. The RC modification allows confirmation that the conclusions will be similar with different RC. The key is using the same RC for all the analysis sequences in the same study.

The first parameter for the analysis sequences is the core material. In the transient analysis, the solver can introduce the total hysteresis data loop from [26] and the material conductivity as input data.

Table 5 shows the material data used in the sequence. The results of the per-unit CPL modifying the material have been are plotted in Fig. 13. There is a clear relationship between the conductivity and the per-unit CPL. However, there is not a defined correlation with other parameters, but there is a small contribution from H_{max}.

Equation (19) was proposed to find a correlation between the per-unit CPL (from ECL) and other equivalent values. This result was obtained by focusing on achieving a good enough and quick approximation (Fig. 14).

$$\frac{P_i}{P_1} = \left(\frac{H_{max\,i}}{H_{max\,1}}\right)^{0.01} \cdot \left(\frac{\sigma_i}{\sigma_1}\right)^{-0.4} \tag{19}$$

A. CORE VOLUME EFFECT
The Per-unit CPL (from core volume) is invariable during the frequency range as usual in this research for the Per-unit CPL
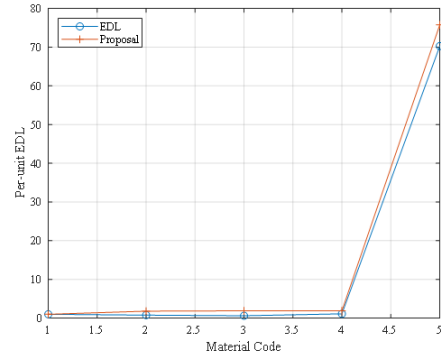

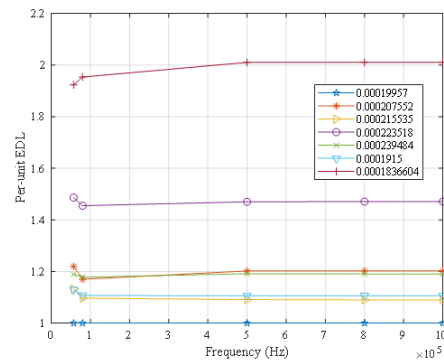**FIGURE 14.** Per-unit EDL vs. material code.

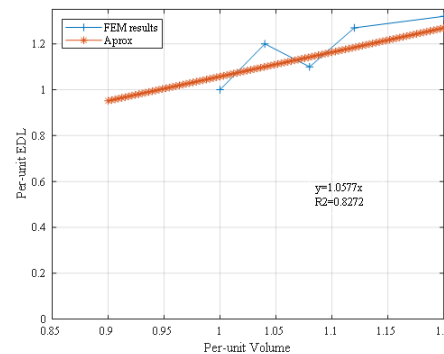**FIGURE 15.** Per-unit EDL vs. f (Core Volume).

FIGURE 16. Per-unit EDL vs. per-unit volume.

(Fig. 15). The Per-unit CPL has been plotted versus the Per-unit Volume, (Fig. 16). Equation (20) defines the correlation between the Per-unit CPL (from ECL) and Per-unit Volume.

$$\frac{P_i}{P_1} \sim \left(\frac{V_i}{V_1}\right)^{1.05} \tag{20}$$

If other analysis sequences to modify the core volume would have developed as in the HL analysis, the same conclusion would have been achieved. The nature of HL is different from ECL because HL is linked to the surface of the hysteresis loop area of the material core and ECL is linked to the component surface area. This assumption can be generalized for every magnetic component in power electronics.
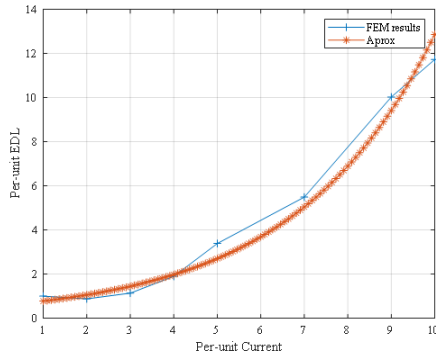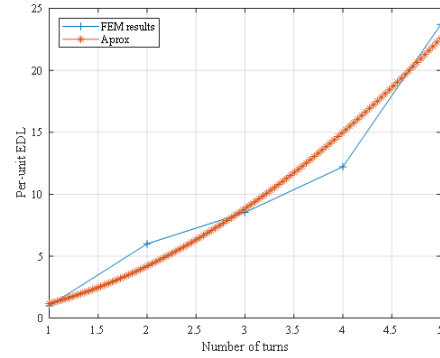
FIGURE 17. Per-unit EDL vs. per-unit current.

FIGURE 18. Per-unit EDL vs. number of turns.

B. WINDING CURRENT EFFECT

Following the same process as for the hysteresis analysis, the winding current and turns number parameters were analysed by sequences. The per-unit ECL was again constant with the frequency in both sequences.

Figure 17 corresponds to the coil current sequence and Fig. 18 corresponds to the winding number sequences, leading to the following relationships:

$$\frac{P_i}{P_1} \sim \frac{1}{2} \cdot \left(\frac{I_i}{I_1}\right)^{1.2} \tag{21}$$

$$\frac{P_i}{P_1} = 1.18 \cdot \left(\frac{n_i}{n_1}\right)^{1.8} \tag{22}$$

C. WINDING POSITION AT THE CORE EFFECT

The lateral distance between windings sequence considers the same lateral distance between them. This assumption is usual in manufacturing design.

In this sequence, several lateral distances were checked. The per-unit CPL had a constant value during the frequency range analysed. There were several configurations that are not usual for power converters, but they were analysed by FEA to achieve a mathematical correlation

The main factor that impacts the ECL was the current loops created due to the magnetic field. Then, the winding position, as expected, did not modify the magnetic field inside the core to a large scale. Consequently, the value of the per-unit CPL (from ECL) has no impact. Even the correlation is equal to that of the HL analysis:

$$\frac{P_i}{P_1} = e^{-0.004 \cdot \alpha} \tag{23}$$

D. WINDING POSITION EFFECT

The main factors, material core, core volume, coil current, and winding number and lateral position, were studied. In the HL analysis, the impact for different potential coil configurations was negligible (i.e.: the distance between the windings and the core), less than around 5% in equivalent terms.

The assumption for ECL analysis about the winding configurations was done considering that it obtained the same conclusions as the HL due to the results of the previous

sections and it was also based on the current on the component surfaces because the magnetic field created by the winding does not change significantly in the different ECL equivalent sequences.

E. EDDY CURRENT LOSS EQUATION

The relationship between P_i and P_1 (the RC for the ECL analysis) for each involved parameter was established. The conclusions obtained permit defining an equation to predict the eddy core loss for toroidal components due to knowing the effect of each parameter. Considering a constant lateral distance between windings and unsaturated status, the ECL, using the correlations determined before that are good approximations for range of frequencies between 1 Hz and 1200 kHz, can be defined as:

$$P_{oe} = \left(13.15 \cdot e^{-0.0004 \cdot \alpha}\right) \cdot \left(n_i^{1.8}\right) \cdot \left(I_i^{1.2}\right) \cdot V \tag{24}$$

$$P_{ie}(f) = P_{oe} \cdot f^{\exp} \rightarrow \exp = 0.18 \left(\frac{H_{\max i}}{H_{\max 1}}\right)^{0.01}$$
$$\cdot \left(\frac{\sigma_i}{\sigma_1}\right)^{-0.4} + 0.1138 \tag{25}$$

where P_{oe} is the EDL for the magnetic component (1 Hz) and P_{ie} is the EDL in the frequency working point desired. The superposition theorem was used similarly to in the HL analysis; this theorem can apply to magnetic fields and current densities [2].

Thus, if the toroidal core component has more than one winding, the ECL defines:

$$P_{oe} = \sum \left(13.15 \cdot e^{0.0004 \cdot \alpha}\right) \cdot \left(n_i^{1.8}\right) \cdot \left(I_i^{1.2}\right) \cdot V \tag{26}$$

$$P_{ie}(f) = P_o \cdot f^{\exp} \rightarrow \exp = 0.18 \left(\frac{H_{\max i}}{H_{\max 1}}\right)^{0.01}$$
$$\cdot \left(\frac{\sigma_i}{\sigma_1}\right)^{-0.4} + 0.1138 \tag{27}$$

VI. METHOTODOLY AND VALIDATION
A. METHODOLOGY

After the completed FEA study, the proposed method to calculate the CPL was divided into several steps since the
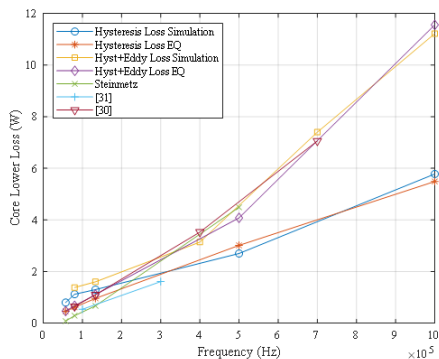
FIGURE 19. Validation. Component I.

TABLE 6. Validation component I (using maxwell).

Core	Winding: 1A	
C107.65.25	3 turns (Lateral distance 4°)	
Material: 3F3	Copper AWG18	

TABLE 7. Validation component II (using pexprt).

Core	Winding: 1A	
TX.10/6/4	5 turns (Lateral distance∼72°)	
Material: 3C92	Copper AWG13	

core is not saturated because the inductive component for switching power supplies works under the knee point, B_{sat}

1) Defining the toroidal core (dimensions) and winding/s configuration/s.
2) Calculating the hysteresis loop area from [26] with polynomial approximation.
3) Applying (17–18) for HL and (26–27) for the ECL in the frequency point of interest.
4) The CPL is the sum of (18) and (27).

B. VALIDATION

Component I (see Table 6) core losses were obtained with the proposed methodology using (19)–(27). The results were compared with a) the experimental measurements made in [30], b) an analytical assessment different from the Steinmetz equation, presented in [31], and c) the CPL of Component I calculated with ANSYS Maxwell [29] using (2–3) where the actual material was simulated and a total of 435635 FE were used. Our results are in a good agreement with the experimental results [30] for 400 to 700 kHz, as shown in Fig. 19. Our results from 100 to 300 kHz match the mathematical results from [31] in an acceptable way. Finally, differences between the simulations and the proposed equations are under 5%.
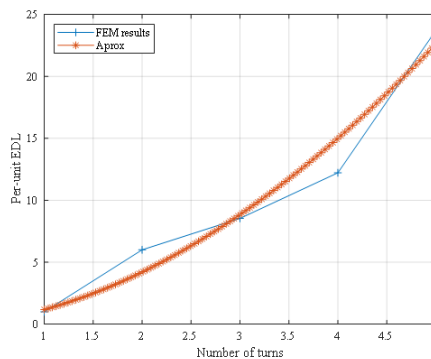

FIGURE 20. Validation. Component II.

The analysis of component II was done using ANSYS PExprt [32] (see Table 7) and compared with the results obtained using the proposed expressions. As shown in Fig. 20, the results obtained using our equations agree with the results obtained from ANSYS PExprt that use the Steinmetz equation for the power core loss calculation. It is important to note that the core material is not in the list of materials used to obtain our equations included in Table 1. This is a sign of the validity of the assumptions made during our developments.

In summary, the obtained results (Figures 19 and 20) demonstrate that the equations are a good approach to calculate the power core loss for toroidal components.

VII. CONCLUSION

An original methodology based on 3D FEM simulation permutations has been described to analyse the power core loss that does not require a previous analysis of magnetic field density.

The concept of the per-unit CPL is useful to compare the values of the losses independent of the frequency and to run the impact analysis for different parameters independently.

The proposed equations give power core loss estimations with an error lower than 5% (compared with the values obtained using Steinmetz equation) helping electronics designers to obtain these losses using only the data given in manufacturer datasheet in the frequency range (1-1200 MHz).

This work also allows splitting the HL and ECL, helping engineers when making design decisions in designing an inductive component to minimize them.

REFERENCES

[1] C. P. Steinmetz, "On the law of hysteresis," *Proc. IEEE*, vol. 72, no. 2, pp. 197–221, Feb. 1984, doi: 10.1109/PROC.1984.12842.
[2] O. Zinke, "Spulen und magnetische Werkstoffe," in *Widerstände, Kondensatoren, Spulen und ihre Werkstoffe*. Berlin, Germany: Springer, 1965, doi: 10.1007/978-3-662-00453-1_3.
[3] R. H. Pry and C. P. Bean, "Calculation of the energy loss in magnetic sheet materials using a domain model," *J. Appl. Phys.*, vol. 29, no. 3, pp. 532–533, Mar. 1958, doi: 10.1063/1.1723212.
[4] G. Bertotti, "Physical interpretation of eddy current losses in ferromagnetic materials. II. Analysis of experimental results," *J. Appl. Phys.*, vol. 57, no. 6, pp. 2118–2126, Mar. 1985, doi: 10.1063/1.334405.

[5] G. Bertotti, "General properties of power losses in soft ferromagnetic materials," *IEEE Trans. Magn.*, vol. MAG-24, no. 1, pp. 621–630, Jan. 1988, doi: 10.1109/20.43994.

[6] T. Kochmann, "Relationship between rotational and alternating losses in electrical steel sheets," *J. Magn. Magn. Mater.*, vol. 160, pp. 145–146, Jul. 1996, doi: 10.1016/0304-8853(96)00145-X.

[7] L. Michalowski and J. Scheinder, *Magnettechnik-Grundlagen, Weksoffe, Anwendugen*, 3rd ed. Essen, Germany: Vulkan-Verlag GmbH, 2006.

[8] J. Reinert, A. Brockmeyer, and R. W. A. A. De Doncker, "Calculation of losses in ferro- and ferrimagnetic materials based on the modified Steinmetz equation," *IEEE Trans. Ind. Appl.*, vol. 37, no. 4, pp. 1055–1061, Jul./Aug. 2001, doi: 10.1109/28.936396.

[9] J. Li, T. Abdallah, and C. R. Sullivan, "Improved calculation of core loss with nonsinusoidal waveforms," in *Proc. Conf. Rec. IEEE Ind. Appl. Conf., 36th IAS Annu. Meeting*, Chicago, IL, USA, vol. 4, Oct. 2001, pp. 2203–2210, doi: 10.1109/IAS.2001.955931.

[10] K. Venkatachalam, C. R. Sullivan, T. Abdallah, and H. Tacca, "Accurate prediction of ferrite core loss with nonsinusoidal waveforms using only steinmetz parameters," in *Proc. IEEE Workshop Comput. Power Electron.*, Mayaguez, PR, USA, Jun. 2002, pp. 36–41, doi: 10.1109/CIPE.2002.1196712.

[11] J. Muhlethaler, J. Biela, J. W. Kolar, and A. Ecklebe, "Improved core-loss calculation for magnetic components employed in power electronic systems," *IEEE Trans. Power Electron.*, vol. 27, no. 2, pp. 964–973, Feb. 2012, doi: 10.1109/TPEL.2011.2162252.

[12] F. Preisach and F. Z. Physik, "Über die magnetische Nachwirkung," *Zeitschrift Phys.*, vol. 94, no. 5, pp. 277–302, 1935, doi: 10.1007/BF01349418.

[13] D. Jiles and D. Atherton, "Theory of ferromagnetic hysteresis," *J. Magn. Magn. Mater.*, vol. 61, nos. 1–2, pp. 48–60, 1986, doi: 10.1016/0304-8853(86)90066-1.

[14] *Flux 10–2D/3D Applications User's Guide*. Cetrat Group, Meylan, France, 2007.

[15] M. Hafner, F. Henrotte, M. H. Gracia, and K. Hameyer, "An energy-based harmonic constitutive law for magnetic cores with hysteresis," *IEEE Trans. Magn.*, vol. 44, no. 6, pp. 922–925, Jun. 2008, doi: 10.1109/TMAG.2007.916141.

[16] D. Eggers, S. Steentjes, and K. Hameyer, "Advanced iron-loss estimation for nonlinear material behavior," *IEEE Trans. Magn.*, vol. 48, no. 11, pp. 3021–3024, Nov. 2012, doi: 10.1109/TMAG.2012.2208944.

[17] D. Linzen and R. W. De Doncker, "Simulation of power losses with MATLAB/simulink using advanced power device models," in *Proc. IEEE Workshop Comput. Power Electron.*, Mayaguez, PR, USA, Jun. 2002, pp. 71–75, doi: 10.1109/CIPE.2002.1196718.

[18] S. Barg, K. Ammous, H. Mejbri, and A. Ammous, "An improved empirical formulation for magnetic core losses estimation under nonsinusoidal induction," *IEEE Trans. Power Electron.*, vol. 32, no. 3, pp. 2146–2154, Mar. 2017, doi: 10.1109/TPEL.2016.2555359.

[19] S. Yue, Y. Li, Q. Yang, X. Yu, and C. Zhang, "Comparative analysis of core loss calculation methods for magnetic materials under nonsinusoidal excitations," *IEEE Trans. Magn.*, vol. 54, no. 11, pp. 1–5, Nov. 2018, doi: 10.1109/TMAG.2018.2842064.

[20] S. Yue, Q. Yang, Y. Li, C. Zhang, and G. Xu, "Core loss calculation of the soft ferrite cores in high frequency transformer under non-sinusoidal excitations," in *Proc. 20th Int. Conf. Electr. Mach. Syst. (ICEMS)*, Sydney, NSW, Australia, Aug. 2017, pp. 1–5, doi: 10.1109/ICEMS.2017.8056411.

[21] L. Yang, Y. Li, Z. Li, P. Wang, S. Xu, and R. Gou, "A simplified analytical calculation model of average power loss for modular multilevel converter," *IEEE Trans. Ind. Electron.*, vol. 66, no. 3, pp. 2313–2322, Mar. 2019, doi: 10.1109/TIE.2017.2779417.

[22] B. Delinchant, F. Wurtz, J. Vasconcelos, and J.-L. Coulomb, "Framework for the optimization of online computable models," *Int. J. Comput. Math. Electr. Electron. Eng.*, vol. 33, no. 3, pp. 745–758, Apr. 2014.

[23] D. S. Kiselev, M. G. Persova, Y. G. Soloveichik, Y. I. Koshkina, D. V. Vagin, and E. I. Simon, "Comparison of approaches and the software for 3D finite element modeling of harmonic electromagnetic fields," in *Proc. 13th Int. Sci.-Tech. Conf. Actual Problems Electron. Instrum. Eng. (APEIE)*, Novosibirsk, Russia, Oct. 2016, pp. 255–258, doi: 10.1109/APEIE.2016.7806463.

[24] P. S. Kumar, "Design of high frequency power transformer for switched mode power supplies," in *Proc. Int. Conf. Emerg. Trends Eng., Technol. Sci. (ICETETS)*, Pudukkottai, India, Feb. 2016, pp. 1–5, doi: 10.1109/ICETETS.2016.7603076.

[25] *Browser FIREFOX*. [Online]. Available: https://www.ansys.com/products/electronics/ansys-maxwell

[26] *Data Handbook of Ferroxcube*, Hispano Ferritas, Guadalajara, Spain, Nov. 2017.

[27] Y. Zhang, M.-C. Cheng, and P. Pillay, "Magnetic characteristics and excess eddy current losses," in *Proc. IEEE Ind. Appl. Soc. Annu. Meeting*, Houston, TX, USA, Oct. 2009, pp. 1–5, doi: 10.1109/IAS.2009.5324814.

[28] R. Asensi, R. Prieto, J. A. Cobos, and J. Uceda, "Modeling high-frequency multiwinding magnetic components using finite-element analysis," *IEEE Trans. Magn.*, vol. 43, no. 10, pp. 3840–3850, Oct. 2007, doi: 10.1109/TMAG.2007.903162.

[29] J. R. Gonzalez, R. Prieto, and R. Asensi, "Simplifications in 3D high-low frequency models of multi-winding magnetic components (EE & toroidal cores)," *Int. J. Magn. Electromag.*, vol. 1, no. 1, pp. 1–7, Dec. 2015, doi: 10.35840/2631-5068/6503.

[30] Y. Han, G. Cheung, A. Li, C. R. Sullivan, and D. J. Perreault, "Evaluation of magnetic materials for very high frequency power applications," *IEEE Trans. Power Electron.*, vol. 27, no. 1, pp. 425–435, Jan. 2012, doi: 10.1109/TPEL.2011.2159995.

[31] C. J. Dunlop, "Modeling magnetic core loss for sinusoidal waveforms," Ph.D. dissertation, Naval Postgraduate School, Monterey, CA, USA, 2008.

[32] *Browser FIREFOX*. [Online]. Available: https://www.ansys.com/products/electronics/ansys-pexprt

JORGE RAFAEL GONZÁLEZ-TEODORO received the master's degree in industrial engineering and the D.E.A. degree in cryogenics from Extremadura University, Badajoz, Spain, in 2006 and 2008, respectively. He is currently pursuing the Ph.D. degree in 3D modeling magnetic components. He has a Lead engineering experience in nuclear engineering and plasma diagnostics systems as well as design integration and multiphysics analysis for fusion machines and accelerators.

ENRIQUE ROMERO-CADAVAL (Senior Member, IEEE) received the M.Sc. degree in industrial electronic engineering from the Escuela Técnica Superior de Ingeniería Industrial (ICAI), Universidad Pontificia de Comillas, Madrid, Spain, in 1992, and the Ph.D. degree from the Universidad de Extremadura, Badajoz, Spain, in 2004. In 1995, he joined the University of Extremadura, where he teaches power electronics and researches within the Power Electrical and Electronic Systems (PE&ES) Research and Development Group, School of Industrial Engineering. He has participated in several projects dealing with power electronics applied to power systems, power quality, active power filters, electric vehicles, smart grids, and renewable energy resources.

RAFAEL ASENSI was born in Madrid, Spain, in 1966. He received the M.Sc. and Ph.D. degrees in electrical engineering from the Universidad Politécnica de Madrid (UPM), Madrid, in 1991 and 1998, respectively. In 1994, he joined the Department of Electrical Engineering, where he is currently an Associate Professor. His research interests include high-frequency modeling of magnetic components and non-linear load modeling and simulation.

• • •